HAL
open science

Change Detection in Floodable Areas of the Danube Delta using Radar Images

Simona Niculescu, Cédric Lardeux, Grégoire Mercier, Laurence David

To cite this version:

Simona Niculescu, Cédric Lardeux, Grégoire Mercier, Laurence David. Change Detection in Floodable Areas of the Danube Delta using Radar Images. SAGEO 2013, Sep 2013, Brest, France. pp.499-519. hal-00991965

HAL Id: hal-00991965

https://hal.science/hal-00991965v1

Submitted on 16 May 2014

HAL is a multi-disciplinary open access archive for the deposit and dissemination of scientific research documents, whether they are published or not. The documents may come from teaching and research institutions in France or abroad, or from public or private research centers.

L'archive ouverte pluridisciplinaire **HAL**, est destinée au dépôt et à la diffusion de documents scientifiques de niveau recherche, publiés ou non, émanant des établissements d'enseignement et de recherche français ou étrangers, des laboratoires publics ou privés.

Change Detection in Floodable Areas of the Danube Delta using Radar Images

Simona Niculescu[1], Cédric Lardeux[2], Grégoire Mercier[3], Laurence David[1]

1.Laboratoire LETG-Brest, Géomer - UMR 6554 CNRS
Rue Dumont d'Urville, Technopole Brest Iroise, F-29470 Plouzané, France
simona.niculescu@univ-brest.fr

2. Office National des Forêts
2, avenue de Saint-Mandé, 75570 Paris Cedex 12
clardeux@gmail.com

3. Institut Télécom, Télécom Bretagne, Lab-STICC/CID - UMR 6285 CNRS
Technopole Brest-Iroise; CS 83818
F-29238 Brest cedex – France
gregoire.mercier@telecom-bretagne.eu

RESUME

Dans le delta du Danube, le risque d'inondation est un risque majeur. Depuis les années 2000, la zone humide côtière du delta a été frappée par des inondations en 2002, 2005, 2006 et 2010. En partant d'une série de données hydrologiques et d'observations satellite de 2009 et de l'été 2010, on utilise dans cet article l'information et les observations sur l'occupation du sol, notamment dans le domaine de l'inondable, pour étudier la problématique de la prévision du risque. L'un des objectifs principaux de la méthodologie développée consiste en la mise en œuvre de différents types de données pertinentes pour ce type d'analyse en proposant une chaîne méthodologique spécifique pour la détection du changement en termes de risque d'inondation. Les données du satellite japonais ALOS sont utilisées pour présenter une démarche méthodologique de traitement de données radar multidates fondée sur une analyse de l'entropie temporelle permettant de détecter des changements dans les zones inondables du delta du Danube.

ABSTRACT

In the wetlands of the Danube delta floodplain, flooding is a major natural risk. Since 2000, the coastal wetland has been seriously impacted by floods in 2002, 2005, 2006 and 2010. Using hydrological and satellite observations acquired in 2009 and during the summer of 2010, this paper tackles the issue of forecasting risk based on land cover information and observations. A major objective of this methodological work consists in exploring several types of data from the Japanese ALOS satellite. These data are used to illustrate a

multitemporal radar data processing methodology based on temporal entropy analysis enabling change detection in the floodable areas of the Danube delta.

MOTS-CLES : *delta du Danube, risque d'inondation, détection du changement, entropie temporelle, satellite ALOS, prévision, zone inondable.*

KEYWORDS: *Danube delta, flood risk, change detection, temporal entropy, ALOS satellite, forecasting, floodable areas*

1.Introduction

Assumptions related to global warming and its effects engender significant preoccupations with regards to the rise in heavy rainfall occurrences despite numerous doubts that still exist concerning rainfall response to global warming. In this respect, climate change may increase flooding and other risks throughout the whole water cycle in the years to come. Extreme weather conditions such as heavy rains causing flash floods are expected to become more frequent throughout Europe. Climate change is also expected to lead to a rise in the sea level (expected to be from 18 to 59 cm in 2100, IPCC, 2007) and shoreline erosion and, when accompanied by strong storm waves, will threaten low altitude coastal towns, which will be more likely flooded. According to GIEC, this phenomenon will probably affect up to 1.6 million more Europeans until 2070. The rise in sea level will also be damaging for the coastal wetlands.

The geographical landscape dealt with in this paper refers to deltas, i.e. recently formed ever-changing environments that are part of the shoreline and wetlands and that are influenced by absent or weak tides. These are generally characterized by salinity variations –freshwater from the river on the one hand and marine saltwater on the other hand – as well as by considerable biomass and productivity, due mainly to the abundance of nutrients present in the water and sediments. Despite their indisputable importance, these environments remain among the most endangered ecosystems in the world due to land reclamation, drying out, pollution or overexploitation of resources. The Danube delta, a coastal wetland of the Black Sea, cannot escape these dangers and, to preserve its resources, it has been declared a Biosphere Reserve (in 1993). The Danube delta is a representative flood hazard site since it has been affected by climate-related floods and hence by systematic rises of the water level.

Radar satellites are extremely useful for characterizing and mapping flood risks due to their ability to collect data and images through the cloud cover that usually accompanies floods. The purpose of this paper is to test the Japanese ALOS satellite, specifically the PALSAR microwave radar (*Phased Array type L-band Synthetic Aperture Radar*) with 15 m resolution permitting the discrimination of floodable areas. Change detection by temporal entropy based on radar images is the methodology proposed in this paper.

2. Study area

The Danube crosses Europe from Germany to the Black Sea where it forms the second largest delta in Europe after the one at the mouth of the Volga. The Danube delta area covers 4 455 km^2 and 79% (i.e. 3 510 km^2 without the Razim-Sinoe lagoon complex) of the delta area is located in southeastern Romania (figure 1). The Romanian portion of the delta is divided between the inland water area and the maritime area (figure 1). The inland section is located westward from a line connecting the Letea dunes (Periprava Village) with the Dunavat peninsula. The maritime section begins at the alignment of the Letea Caraorman and Crsanicol marine levees and runs all the way to the Black Sea. Our study site is located around Caraorman: the Caraorman fishing village, where fishermen berth their boats, the village and forest bearing the same name (figure 1). The village was set up on the Caraorman levee, 12 m above sea level.

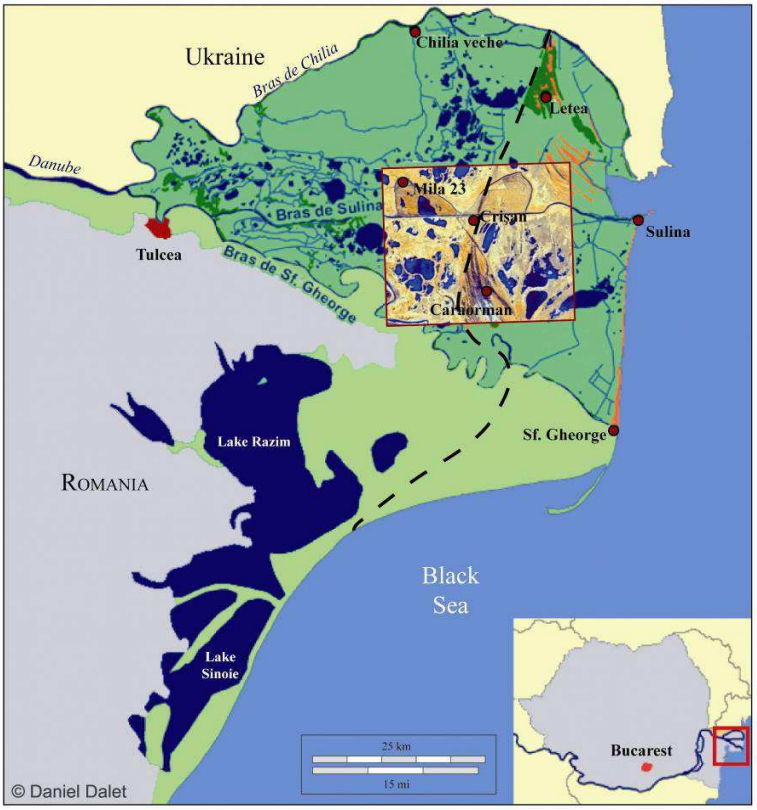

Figure 1. The Danube delta and geographical location of the training sample

At the outset, the hydrographic network of the delta is formed by three main arms: the Chilia arm (120 km long), which forms the natural border between Romania (south) and the Ukraine (north), the Sulina arm (64 km long) in the middle and the Sfantu-Gheorghe arm to the south, currently 70 km long. The delta plain is characterized by minor altitude differences: 20.5% of the delta is below the 0 level of the Black Sea, 54.6 % is between 0 and 1 m, 18.2% is between 1 and 2 m and only 6.7% is above 2 m of altitude. The low-lying areas between the Chilia-Sulina and Sulina-Sfantu-Gheorghe arms harbor many delta lakes taking up 8.9% of the whole delta area (Gastescu P. and Stiuca R., 2008). These lakes play an important role during rises in the Danube level, as the excess water accumulates here and then flows into the main arms when the water level is low. Another characteristic of this deltaic environment is the existence of ecosystems consisting of reed beds, mainly *Phragmites australis*. These reed beds make up a considerable part of the floodable delta and they are also thought to be the largest uninterrupted reed beds in the world.

Despite the moderate rainfalls in this area, the Danube delta is flooded every year. The historical analysis of the maximum discharge of the Danube (figure 2) in Tulcea reveals that considerable river discharges were recorded in 1895 (13 700mc/s), 1942 (13 387mc/s), 1970 (14 520mc/s), 1974, 2003, 2006 (15 900 mc/s) and 2010 (16 600mc/s). The annual multi-analysis (1931 – 2011) of the Danube water levels at the entrance of the delta (in Tulcea) (figure 2) also shows that most of the maximum river discharge episodes occur from March to July. The last two major flood rises, which occurred in 2006 and 2010 (figure 2), were preceded by heavy snowfalls during the winter and by relatively early snow melting on the mountains in the catchment area of the Danube. In July, the Danube level decreases significantly down to low levels and discharge rates at the end of summer and beginning of autumn (from August to February) (figure 2). According to these data, the floods of 2006 and 2010 were followed by periods of considerable low water (figure 2): in Tulcea, the Danube level was 1 m in August 2007 and 0.35 m in October 2011.

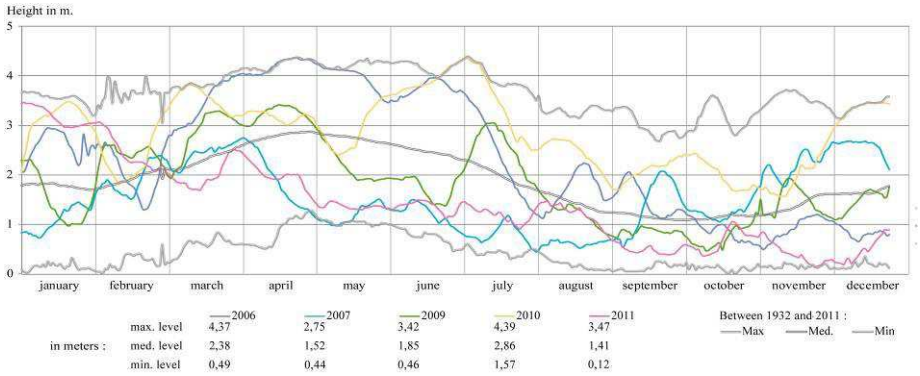

Figure 2. Danube daily levels at Tulcea in 2006, 2007, 2009, 2010 and 2011. Mean daily levels from 1931-2011.

The floods of 2010 affected more than 30 counties and 400 localities in the northern and eastern portions of Romania, the Danube delta included. More than 16 500 people were evacuated and more than 45 000 hectares of agricultural land and forests were submerged.

3. Data set

The satellite data included in this paper were acquired by the PALSAR instrument on the ALOS satellite. The Phased Array type L-band Synthetic Aperture Radar (PALSAR) is an active microwave sensor using the L-band frequency (24 cm) to achieve cloud-free and day-and-night land observations. PALSAR is a fully polarimetric instrument, operating in fine-beam mode with single polarization (HH or VV), dual polarization (HH+HV or VV+VH), or full polarimetry (HH+HV+VH+VV). This paper focuses on dual polarization data (dual HH and HV mode) (table 1).

The dual polarimetric mode allows image acquisition in two different linear polarization modes. The alternation between the two polarization configurations occurs on each individual impulse, which accounts for the phase difference between the two acquisitions.

Table 1. ALOS/PALSAR satellite data used

RADAR sensor instrument	Before / during / after the floods	Radar data	Technical characteristics	Danube water level at Tulcea
Japanese ALOS satellite PALSAR sensor	Before	15 June 2009	Dual mode: HH, HV L-Band: 24 cm Resolution: 15 m x15 m	2.52 m
		20 May 2010		3.70 m
	During	18 June 2010		4.37 m
	After	3 August 2010		3.06 m

Other types of data were used: the daily Danube levels in Tulcea in 2006, 2007, 2009 and 2010, the multi-annual mean of the Danube levels in Tulcea between 1931 and 2011, as well as the phenological reed calendar in the Danube delta (figure 5).

4. Methods

In order to detect the various types of surface changes resulting from the floods of 2010 in the Caraorman deltaic section and to characterize the floodable class by means of its backscattering mechanisms, we propose the following methodological analysis and image processing sequence: polarimetric indices extraction and implementation, calculation of the temporal entropy of the polarimetric indices, temporal entropy classification using support vector machine (SVM) and mono temporal floodable class classification using all the polarimetric indices (table 2) used.

Dataset		Danube water levels at Tulcea		Processing steps	Image processing	Objectives
Radar Dataset ALOS / PALSAR	06/15/2009	Normal condition (June 2009)	2.52 m	**Orthorectification** **Data filtering** **Polarimetric indices** **Temporal entropy of the polarimetric indices**	Extraction of the polarimetric indices (intensity) Calculation of the temporal entropy of the polarimetric indices Detection of change entropy of the polarimetric indices	Analysis of polarimetric change between the 2 dates Change indicators (entropy) applied to polarimetric indicators Change characterization (stable classes, changing classes)
	06/18/2010	Floods (June 2010)	4.37 m			
	Image resulting from temporal entropy			**Entropy SVM classification**	Classification into two classes: no change and radical change	Risk class detection (floodable areas): hydrophilic vegetation, halophilic vegetation psamophilic vegetation Stable class mask
	06/15/2009	Normal condition (June)	2.52 m	**Mono-temporal SVM classification**	Diachrony of the 4 dates	Floodable area detection based on the thematic mask extracted relying on the flooded areas of 18 June 2010 (Short vegetation (grassland), hydrophilic vegetation, psamophilic vegetation, mixed vegetation, mixed phragmites, forest, doinant phragmites, cut phragmites)
	05/20/2010	Flood onset	3.70 m			Flooded area detection
	06/18/2010	During	4.37 m			Flooded area detection and thematic mask of these areas
	08/03/2010	After	3.06 m			Floodable area detection and characterization

Table 2: Methodological sequence applied to ALOS/PALSAR images

Two major types of polarimetric indices can be extracted from fully polarized data or from dual polarization data. Coherent indices conserve the phase information while incoherent indices break up the phase information common to the resolution cells. The parameters of interest in these areas for radar modeling are basically the parameters describing the geometry and electromagnetic features of the ground vegetation and soil elements. Thus due to the incoherent nature of the study classes we will focus only on incoherent polarimetric indices.

Polarimetry relies on the vector-like nature of the wave (Papathanassiou and Cloude, 2001). It is designed to characterize targets by recording their responses in different radar wave emission and reception polarizations. In order to allow the separation of backscattering mechanisms in the same resolution cell, different target decomposition models were proposed (Touzi et al. 2002; Lee and Pottier, 2009). Their principle relies on polarimetric data projection on canonical bases associated with each type of backscattering mechanism resulting from the interactions between the radar waves and the excited targets. These methods differ depending on the coherent or incoherent nature of the targets. As far as coherent targets are concerned, we should mention Pauli decomposition (Cloude and Pottier, 1997), SDH decomposition (Krogager, 1999) and Cameron decomposition (Cameron et al., 1996). On the other hand, Cloude-Pottier (Entropie/Alpha), Van Zyl (Van Zyl, 1989, Cloude and Pottier, 1997), Freeman (Freeman and Durden, 1998) and Yamaguchi (Yajima et al, 2008) decompositions describe the non-coherent features of the so-called distributed targets (Cloude and Pottier, 1997; Touzi, 1997).

As for double polarization (fine beam dual mode), only the S_{hh} and S_{hv} terms are recorded coherently, thus reducing the polarimetric information acquired.

Starting from the K_{DP} target vector, the covariance matrix is expressed as:

$$K_L = \begin{pmatrix} Shh \\ Shv \end{pmatrix} \tag{1}$$

$$C = K_L \,.\, K_L{}^* = \begin{pmatrix} Shh \\ Shv \end{pmatrix} \begin{bmatrix} Shh^* \,.\, Shv^* \end{bmatrix} = \begin{bmatrix} Shh\ Shh^* & Shv\ Shh^* \\ Shh\ Shv^* & Shv\ Shv^* \end{bmatrix} \tag{2}$$

$$Shh \,.\, Shh^* = Ahh \,.\, e^{j.\varphi hh} \times Ahh \,.\, e^{-j\varphi hh} = Ahh^2 \,.\, e^{j(\varphi hh - \varphi hh)} = Ahh^2 \,.\, e^0 = Ahh^2 \tag{3}$$

$$Shh = Ahh \,.\, e^{j\varphi hh}$$

$$Shv = Ahv \,.\, e^{j\varphi hv} \tag{4}$$

Shh and Shv are the matrix terms corresponding to HH and HV polarizations. Ahh and Ahv are the amplitudes of the two polarizations, whereas φhh and φhv are their phase.

This configuration allows to extract the coherence degree of HH-HV polarizations as well as the $H_{DP}/A_{DP}/\alpha_{DP}$ parameters (S. Cloude, 2007).

By pointing out that polarimetric ***entropy H*** characterizes the level of depolarization of the backscattered wave, entropy is calculated pixel by pixel using a linear combination of the image cross-variance matrix values.

$$\boldsymbol{H_{DP}} = -\sum_{i=1}^{2} \boldsymbol{P_i log}\ (\boldsymbol{P_i}) \tag{5}$$

Where $\boldsymbol{P_i} = \frac{\lambda i}{\sum_{i=1}^{2} \lambda i}$ and λi are the specific vectors of the coherency matrix.

In a second stage, the temporal analysis of some polarimetric indices (HH intensity, hv intensity and polarimetric entropy) using temporal entropy is carried out using this equation.

$$H_{Temp} = -\sum_{i=1}^{n} \mathbf{P_i} \boldsymbol{log}\ (\mathbf{P_i})$$

Where $\boldsymbol{P_i} = \frac{Bi}{\sum_{i=1}^{n} Bi}$ and bi correspond to the b indicator (HH, HV or polarimetric entropy in our case) observed on date n.

Therefore, temporal entropy has the same definition as polarimetric entropy, the only difference being that temporal entropy measures the changes undergone by the same index throughout time.

Thus, a low temporal entropy (close to 0) means that the indicator used is stable in time. On the other hand, a high entropy value, close to 1, shows that the indicator has undergone a significant change through time.
Moreover, we suggest a comparison between the temporal HH, HV polarization entropies and their polarimetric entropy in order to be able to characterize their changes. It is well known that HH polarization allows the characterization of the double rebound importance where HV polarization is particularly characteristic of the volume reflections. Thus, the temporal analysis of these polarizations together with the analysis of their polarimetric entropy will enable us to characterize the Danube water level evolution. Since the Danube delta is mainly covered by reeds, the water level variation and the reed density variation are characterized by a significant double rebound modulation and volume backscattering mechanism.
Thus, the temporal analysis of HH and HV entropy reveals values that can characterize the state of the changes affecting the studied areas. In some areas, before the floods of 18 June 2010, HH intensity was -7.7dB whereas HV intensity was -15.5. During the floods, HH intensity was -12.5dB versus -26.7dB for HV polarization. This shows that intensity decreases during flooding, which means that water response increases contrary to volume and double bounce scattering mechanisms. Therefore in the delta we can observe many different temporal signatures explained in figure 4 from the Results and discussion chapter

A change detection process was also conducted. Several authors have published change detection method assessments, for instance Singh (1989), Lunetta and Elvidge (1998), Mas (2000), Jensen (2004) and Lu et al. (2004), Inglada and Mercier (2007), Quin, Pinel-Puysségur, and Nicolas (2012).

Lu et al. (2004) classify the change detection methods into six categories: algebraic, transformation, classification, advanced, GIS approach, visual analysis and other techniques.

Therefore, we used the supervised SVM classification algorithm in addition to temporal entropy analysis in order to detect changes and to isolate and characterize the type of area subjected to flooding.

A supervised classification algorithm was then applied. The algorithm used was SVM (*Support Vector Machine*) based on the core theory, which allows the settlement of problems linearly inseparable. It also allows the taking into consideration of numerous heterogeneous parameters. The purpose of the SVM algorithm is to calculate the best hyperplane separating two classes or, similarly, to maximize the margin between the study classes, more details are given in Burges C-J, 1998. Thus, SVM are particularly relevant because SVM do not take into account any distribution assumption. In addition, using kernel RBF[1] of SVM allow classifying non linear classification problem.

The presence of noise in the data can be taken into account by defining a distance allowing a certain data dispersion, thus relaxing the decision-making constraint (Lee J. S., Grunes M. R, de Grandi G., 1999; Lee et al., 2009).

The SVM principle was developed for a two-class problem, yet it may be extended to a higher number of classes according to the "one against one" (OAO) algorithm. This algorithm consists in the development of $\frac{Q(Q-1)}{2}$ hyperplanes separating each pair of classes. The final label is the one that was most commonly retained.
Whereas Q is the number of classes to consider, the UCT algorithm consists in the development of Q hyperplanes separating each class from the others $Q-1$.
As for the core used by the SVM method, please note that after several tests, better results are obtained with the same parameterization as Fukuda and Hirosawa, 2001, with a RBF kernel, with $\sigma = 0.5$ and a cost parameter equal to 1000.

5. Results and discussion

Using two color composites (figures 3), combining HH and HV intensity with entropy, we propose the calculation of the entropy between two images, the first acquired on 15 June 2009 and the second on 18 June 2010 (figure 3), in order to detect the changes that occurred between the two dates. The 2009 date was chosen for improved mapping and comparison between the floodable class and the flooded class of 2010.

[1] The Radial Basis Function (RBF) kernel.

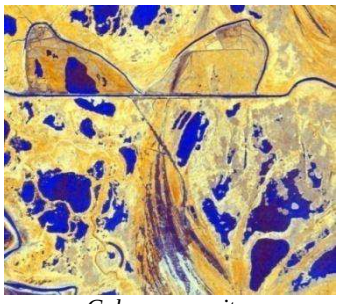

Color composites of June 15, 2009

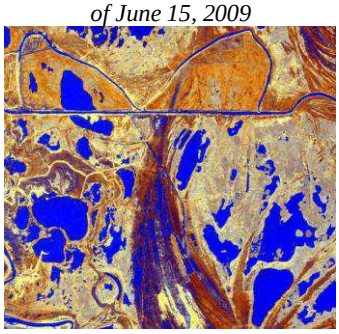

Color composites of June 18, 2010

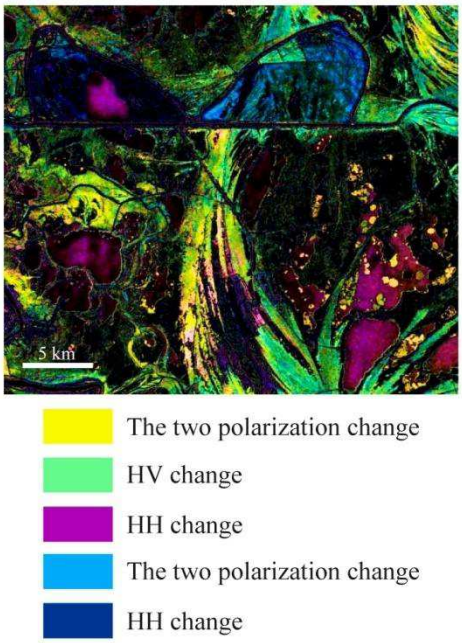

Figure 3. Temporal entropy. Change detection between June 15, 2009 and June 18, 2010.

On the resulting image (figure 3), the lighter the colors, the more numerous the changes recorded. Therefore, yellow expresses a large number of changes, indicating that the two polarizations change, green indicates a HV polarization change, whereas magenta reveals a stable HV polarization and a considerable HH change. Cyan indicates a change in the two polarizations and blue expresses HH change as compared to HV. Bearing in mind that polarimetric information is closely related to the backscattering mechanism, the changes actually reflect the backscattering mechanism changes depending on the changes affecting the studied areas (figure 4).

In order to better characterize the backscattering mechanism and hence to detect changes occurring in these areas depending on the Danube level changes and on the ground vegetation changes (*Phragmites spp.* in particular) before and during the floods, we propose an analysis of the major changes between the two polarizations in the various color composites (figure 4). The different colors used in this diagram correspond to the colors shown in figure 3 (temporal entropy).

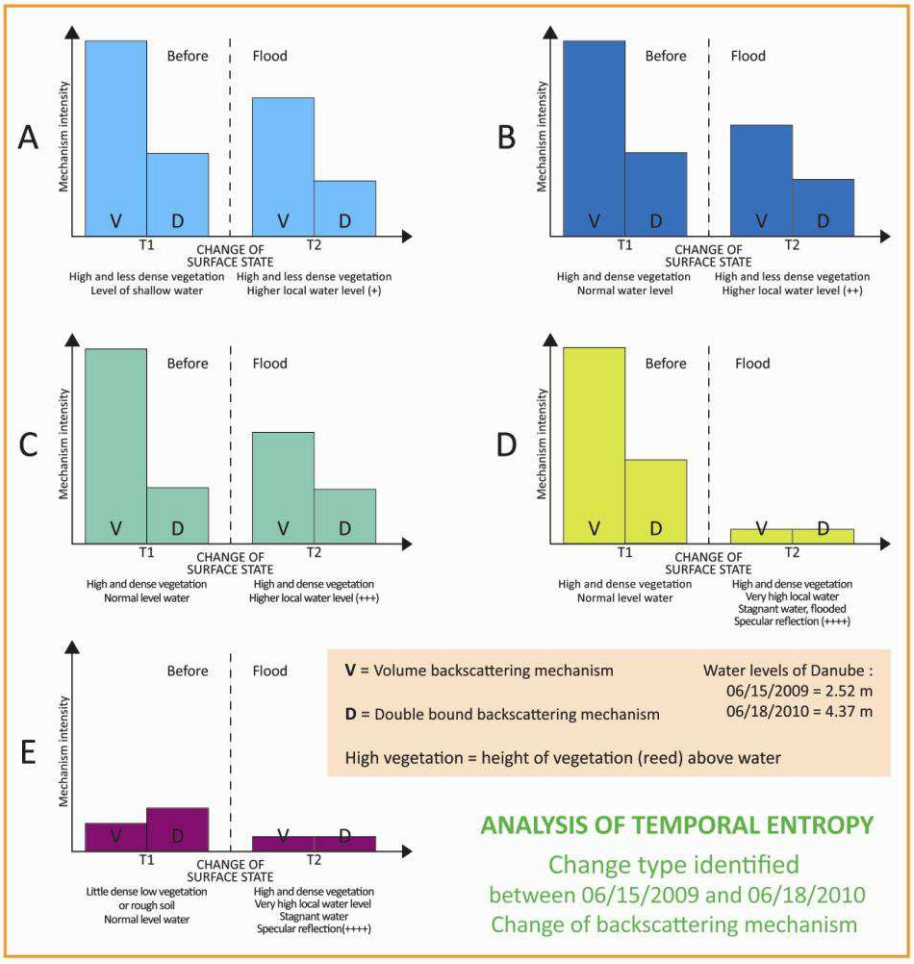

Figure 4: Analysis of temporal entropy

Relying on the field knowledge acquired in connection with the monitored areas and with the characteristics of volume backscattering and double data rebound in double polarization mechanisms, we distinguished between two types of areas in our analysis: the local water level and the vegetation. As far as the changes in the two polarizations (HH and HV) is concerned, which appears here in cyan blue (diagram A), the volume backscattering and double rebound mechanisms are more significant for the date prior to the floods. The areas associated with these backscattering mechanisms are the high and less dense vegetation and the low water level (2.5m), and the high and less dense vegetation and the higher local water level (+), respectively. The changes in the HH polarization as compared to the HV polarization, in blue (diagram B), is somewhat similar to the previous one, except for double rebound backscattering prior to the events, which is lower than the one recorded when the two polarizations changed (before and during the process). HV

polarization change, in green (diagram C), is characterized by considerable volume backscattering prior to the events, which decreases during the process (less than 50% compared to the one prior to the events). As for double rebound backscattering, it is about 30% lower than the volume backscattering prior to the events and more than 20% higher than the double rebound backscattering during the events, when the local water level is also higher (++). The two mechanisms occurring during the floods characterize a higher local water level (+++). Changes in both the volume backscattering and double rebound polarizations are equal during the floods and distinctly lower than the previous mechanisms and they characterize a very high local water level (the still water of the flooded areas) (diagram D in yellow). The changes in the HH polarization compared to the HV polarization, which remains stable, in magenta (diagram E), show very low volume backscattering prior to the events, when the vegetation is low and less dense, the soil is rough and the water level is normal. During the events, these changes are similar to the changes in the two polarizations in the same environmental conditions (high and dense vegetation and very high water level (++++)).

Reeds are an essential component of the deltaic landscape and *Phragmites australis* is the dominant species in the entire Danube delta. It is also accompanied by other hydrophilic species[2]. The combination of these plants varies and there are different plant communities. Hanganu *et al.* (2002) defined four main communities[3] that differ depending mainly on the soil types, pH, flooding conditions and salinity. The ecological dynamics of the reed beds can be characterized by several types of plant cover, each enjoying its own dynamics in the ecological sequence process. This process is mainly driven by the water levels, as it may be accelerated or stopped by events such as floods (2006, 2010) or drying outs (2007, 2011). The reeds studied by ALOS on June 15 and June 18 were in their development, regeneration and blooming stages (figure 5). The water level in Tulcea was 2.52 m on 15 June 2009 and 4.37 m on 18 June 2010.

[2] Typha angustifolia, Schoenoplectus lacustris, Sparganium sp. and Thelypteris palustris.

[3] Phragmitetum communis, Scipo-Phragmitetum, Bolboschoeno-Phragmitetum and Astero tripolii-Phragmitetum.

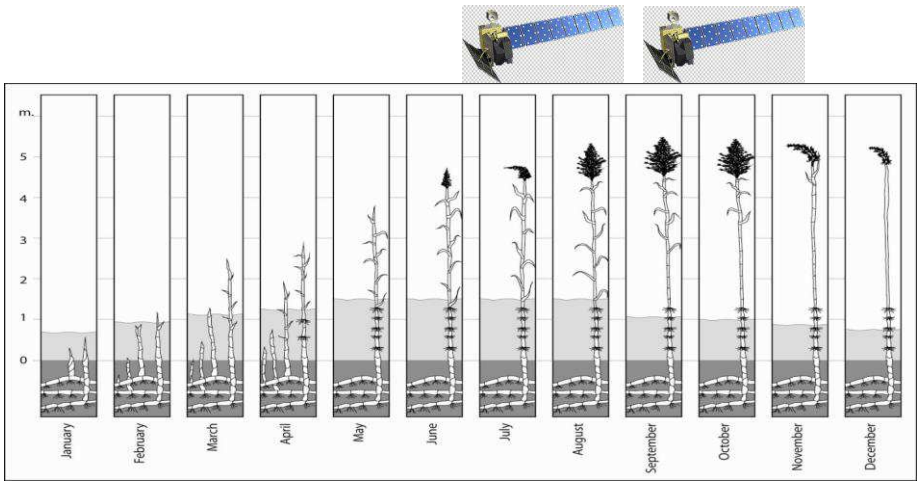

Figure 5. Correspondence between our ALOS data and the reed calendar in the Danube Delta

In a second phase, Support Vector Machine classifications are first applied to temporal entropy in order to extract 3 different classes characterizing change detection (gray and blue classes on next figure). Secondly, in order to determine thematic classes that are affected by flood, we apply an SVM classification for each PALSAR data base only on trained classes of 2009. Thus, the SVM model defined for this date could be applied to the other PALSAR data because PALSAR calibrations are well know to be good and also because we used exactly the same processing chain for each date. The stable classes (forest, delta lakes, cut phragmites, dominating phragmites) are well detected, whereas the flooding classes change the most (short vegetation (grasslands), mixed vegetation, hidrophilic vegetation, psamophilic vegetation, halophilic vegetation). The flooded class is also well illustrated by this image (figure 6).

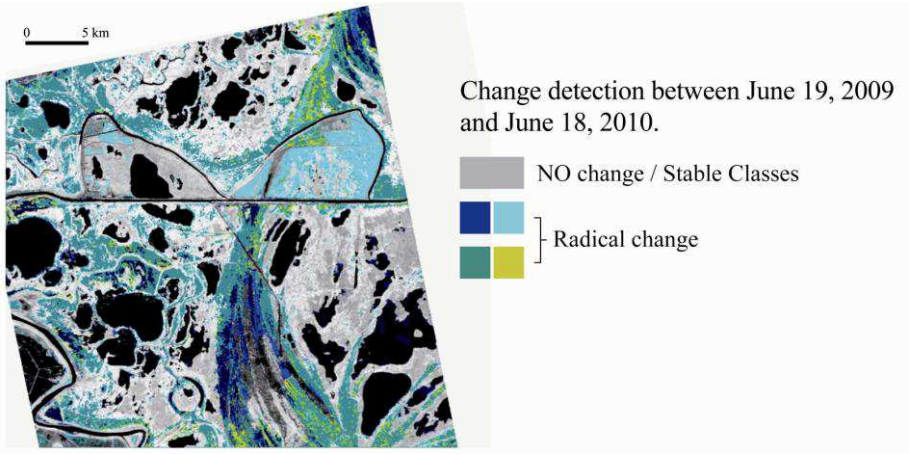

Figure 6. Change detection between June 15, 2009 and June 18, 2010

The more dynamic classes, such as the flooded and floodable classes, are approached through the diachronic analysis of the three dates considered important for these floods: 20 May 2010, 18 June and after the events of 3 August 2010 (figure 8). The date of 15 June 2009 is used to define the floodable classes in relation to the thematic mask of the flooded areas extracted from the image of June 18, when the floods reached their spatial extent peak. June 18 saw the widest flooded areas, especially in Caraorman Village, floods that were mainly due to groundwater oversaturation (rainfall floods). Therefore, as stated before, reference maps for each date were drafted, which suggested the same land cover classes (8 classes) (table 4). Differences between dates were recorded due to the fact that the local water level changed considerably between the four dates. The same thematic classes were used (table 4) but the water level altered the polarimetric response, which accounts for the differences between the floodable classes on certain dates (for instance, June 15, 2009 includes several classes in the floodable areas). Therefore, thematic masks of the floodable areas were extracted for each date and inserted into an image representing the mean of the intensity values on the dates taken into consideration (figure 7).

June 15, 2009. May 20, 2010.

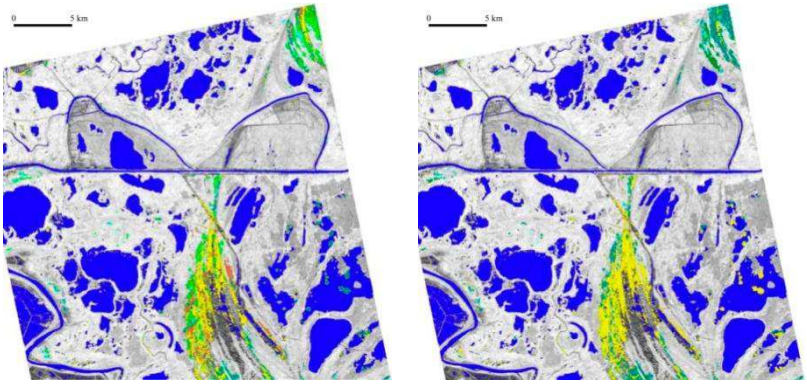

June 18, 2010. August 3, 2010.

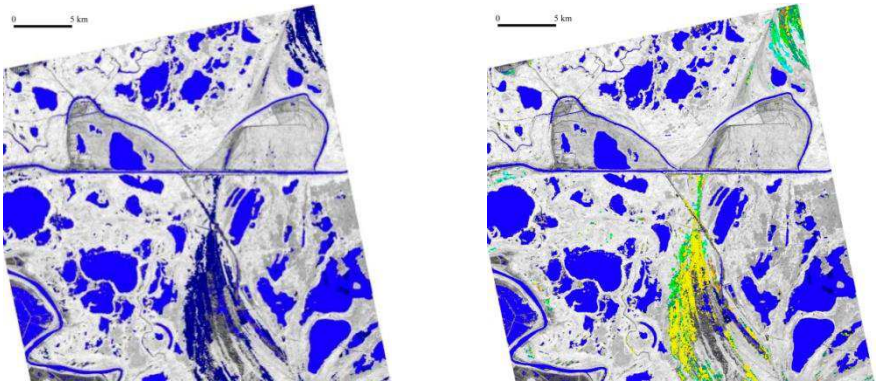

Hydrophilic vegetation

Mixed vegetation (shrubs, hydrophilic vegetation...)

Short vegetation (grassland)

Figure 7. Diachronic evolution of the four dates: before, during and after flooding. The three images acquired prior to and after the floods represent the floodable classes according to the flooded thematic mask extracted from the image of June 18, 2010. The stable classes are in grey.

Examination of the different color composites permitted the definition of classes of interest for flooded and floodable class identification (table 2). We identified a forest class within the stable entropy classification classes, a mixed phragmites class that is also included in the stable classes, a less dense class represented by short vegetation included in the floodable class and classes that changed considerably between 15 June 2009 and 18 June 2010. Other land cover floodable classes were identified: the dunes and interdune depressions, hydrophilic vegetation (Typha, Carex), psamophilic vegetation (Euphorbia), halophilic vegetation (Salicornia). These classes were correlated with the flood classes and the floodable areas (table 3).

Table 3: Correspondence between classification results and flood classes

Classes	**Description**
Submerged: lakes, branches, canals	Permanent waters
Flooded	Flooded between May 20, 2010 and June 8, 2010
Floodable	Short vegetation (grassland), hydrophilic vegetation, psamophilic vegetation, mixed vegetation, mixed phragmites, forest, dominant phragmites, cut phragmites
Drained until August 3, 2010	Flooded on June 18, 2010 and drained until August 3, 2010

The creation of training and control point sets is the result of a random stratified sampling based on the whole set of areas of interest initially determined. 500 training points and 800 control points are set for each class. Results shown in table 4 reveal a very good performance of 95% for the water class, hence the interest for flood monitoring uses. We noted some overlap between short vegetation and mixed vegetation classes, where the performance does not exceed 82%. All the other classes show good performance levels (above 82%), the mean being 87%.

Table 4. Classification performance

Class	Accuracy (percent)
Forest	89
Lake	95
Mixed phragmites	94
Short vegetation	82
Typha_sp	87
Mixed vegetation	82
Cut phragmites	85

Dominant phragmites	84
Mean accuracy	87

Furthermore, work in progress leads us to believe that the performance attained by double polarization radar images in L band (PALSAR) in this study is superior to the performance obtained by optical imaging. The L band wave penetration capacity is particularly suitable for water level variation detection even underneath vegetation cover, such as reeds in the Danube delta. On the other hand, optical imaging only allows the detection of the response of the analyzed area and hence it is not directly sensitive to water level variation.

6. Conclusion and perspectives

This paper provides a methodology for detecting changes using temporal entropy applied to the evaluation of flooded and floodable areas during the Danube delta floods of 2010. Changes were examined at the shortest possible time intervals before and after a flood. These application examples suggest that change detection is possible and could play a fundamental role in the process of understanding, in a broad sense of the term, the temporal evolution of a flooded or floodable landscape via sequential analysis.

Temporal entropy calculated from polarimetric indices is an easy way of detecting changes in the areas under investigation and their comparison makes it possible to conduct a relevant qualitative analysis. Consequently, the analysis of the studied areas enabled us to detect the information most closely related to the changes of interest and least dependent on spatial variations (water level and plant cover). The use of SVM to classify change detection and to characterize the land cover, using respectively temporal entropy and polarimetric indices for each acquisition revealed the major contribution of the land cover based on floodable area classification. The use of polarimetric data helped in the detection of structural differences between the various hydrophilic plant covers and, thus, contributed to the mapping of these types of areas in relation to the water level. It also provided additional information on the spatial extent of the flooded areas.

As far as the future perspectives of our work are concerned, and in order to investigate wavelength influence for flood detection, we intend to conduct a multitemporal full polarization RADARSAT-2 data analysis. In addition, it may be interesting to draw a comparison between dual PALSAR wavelengths (L-band) and RADARSAT-2 wavelengths (C-band), and to document the complementarity of the two instruments/sensors used to detect the land cover of the floodable areas.

References

Burges C-J, 1998, *A tutorial on support vector machines for pattern recognition*, Data mining and knowledge discovery, U. Fayyad, Ed. Kluwer Academic, pp. 1-43.

Cameron, W.L., Youssef, N., and Leung, L.K., 1996, Simulated polarimetric signatures of primitive geometrical shapes, *IEEE Transactions on Geoscience and Remote Sensing*, vol. 34, no. 3, p. 793–803.

Cloude, S. R. and Pottier, E., 1997, A review of target decomposition theorems in radar polarimetry, *IEEE Transactions on Geoscience and Remote Sensing*, vol. 34, no. 1, pp. 68-78.

Cloude S., 2007, The Dual Polarization Entropy/Alpha Decomposition: A PALSAR Case Study. Proceedings : January 2007, Frascati, Italy.

Freeman, A. and Durden, S. L., 1998, A three-component scattering model for polarimetric SAR data, *IEEE Transactions on Geoscience and Remote Sensing*, vol. 36, no. 3, p. 963–973.

Fukuda, S. and Hirosawa, H., 2001, Support vector machine classification of land cover: application to polarimetric SAR data. *Geoscience and Remote Sensing Symposium*. 1, 187-189.

Gastescu P., Stiuca R., *Delta Dunarii. Rezervatie a biosferei*, Edition CD PRESS, 2008, 400p.

Rapport de synthèse GIEC, *Bilan 2007 des changements climatiques*, publié par le Groupe d'experts intergouvernemental sur l'évolution du climat.

Hanganu J., Dubyna D., Zhmud E., Grigoraş, I., Menke U., Drost H., Sefan N., Sarbu, I., 2002, *Vegetation of the Biosphere Reserve "Danube Delta* - with Transboundary Vegetation Map on a 1:150,000 scale, Danube Delta National Institute, Romania; M.G. Kholodny - Institute of Botany & Danube Delta Biosphere Reserve, Ukraine and RIZA, The Netherlands. RIZA report 2002.049 2002, 89 pp.

Inglada J. and Mercier G., 2007, A New Statistical Similarity Measure for Change Detection in Multitemporal SAR Images and its Extension to Multiscale Change Analysis, *IEEE Transactions on Geoscience and Remote Sensing*, vol. 45 (5) pp 1432--1446.

Krogager, E., 1999, New decomposition of the radar target scattering matrix. *IEEE Transactions on Geoscience and Remote Sensing*, vol. 26, no. 18, p. 1525-1527.

Lee J. S., Grunes M. R, de Grandi G., 1999, Polarimetric SAR speckle filtering and its implication for classification. *IEEE Transactions on Geoscience and Remote Sensing*, vol. 37, no. 5, 2362-2373.

Lee, J.S. and Pottier, E., 2009, *Polarimetric radar imaging: from basics to applications*, Brian J. Thompson, New York.

Papathanassiou, K. P. and Cloude, S. R., 2001, Single-baseline polarimetric SAR interferometry. *IEEE Transactions on Geoscience and Remote Sensing*, vol. 39, no. 11, p. 2352–2363.

Quin G., Pinel-Puysségur B, and Nicolas J.-M., 2012, Comparison of harmonic, geometric and arithmetic means for change detection in SAR time series, *EUSAR. 9th European Conference on Synthetic Aperture Radar*, 2012.

Touzi, R., 1997, Target scattering decomposition in terms of roll invariant target parameters, *IEEE Transactions on Geoscience and Remote Sensing*, vol. 45, no. 1, p. 73–84.

Touzi, R. and Charbonneau, F., 2002, Characterization of target symmetric scattering using polarimetric, SAR. *IEEE Transactions on Geoscience and Remote Sensing*, vol. 40, no. 11, p. 693-711.

Van Zyl, J.J., 1989, Unsupervised classification of scattering behavior using polarimetric data, *IEEE Transactions on Geoscience and Remote Sensing*, vol. 27, no. 1, pp. 36-45.

Yajima, Y., Yamaguchi, Y. Sato, R. Yamada, H. and Boerner, W.-M., 2008, PALSAR Image Analysis of Wetlands Using a Modified Four-Component Scattering Power Decomposition, *IEEE Transactions on Geoscience and Remote Sensing*, vol. 46, no. 6, p. 1667-1673.